JOURNAL OF CATALYSIS 129, 130–144 (1991)

A Fourier Transform Infrared Spectroscopic Study of CO_2 Methanation on Supported Ruthenium

MICHAEL R. PRAIRIE,*,[1] ALBERT RENKEN,* JAMES G. HIGHFIELD,†,[2]
K. RAVINDRANATHAN THAMPI,‡ AND MICHAEL GRÄTZEL‡

*Institute for Chemical Engineering, †Laboratory of Technical Chemistry, ‡Institute for Physical Chemistry, Swiss Federal Institute of Technology, CH-1015, Lausanne, Switzerland

Received July 5, 1990; revised December 19, 1990

Diffuse-reflectance infrared Fourier transform (DRIFT) spectroscopy has been used to study *in situ*, the low-temperature ($T < 200$°C) methanation of CO_2 over Ru on TiO_2 supports and on Al_2O_3. For 3.8% Ru/TiO_2, the reaction exhibits an activation energy (E_a) of 19 kcal/mol, is 0.43 ± 0.05 (approximately one-half) order in H_2 concentration, and essentially independent of CO_2 concentration. At 110°C, 40% of the available metal sites are occupied by CO ($\theta_{CO} = 0.4$), a known methanation intermediate. In contrast to Ru/TiO_2, Ru/Al_2O_3, despite having the same E_a and $\theta_{CO} = 0.2$, is 15 times less active. Batch catalyst screening experiments showed no dependence of methanation activity on adsorbed CO (CO_a) formation rate (as modeled by HCOOH dehydration) or on θ_{CO}. In view of this, and the fact that CO dissociation is known to be structure-sensitive, heterogeneity in the active sites is invoked to reconcile the data. The high Ru dispersion on TiO_2 is believed to contribute to the enhanced activity over this support. Adsorbed CO_2 and H_2 react, possibly at the metal-support interface, to form CO_a via rapid equilibration of the reverse water–gas shift reaction, in which HCOOH (and/or $HCOO^-$ ion) play a major role. According to this view, the CO_a and $HCOO_a^-$ intermediates seen by FTIR represent accumulated reservoirs en route to CH_4, in which the CO_a hydrogenation step is rate-controlling. An interesting synergy occurs for mixtures of Ru/anatase and Ru/rutile, the former being a better catalyst for CO_a supply while the latter is more effective in CO_a hydrogenation.

INTRODUCTION

Recently we described a 3.8% Ru/TiO_2 catalyst that exhibits very high activity for CO_2 methanation and photo-assisted rate enhancement (*1, 2*). In this paper, we present results from our ongoing research aimed at understanding why the catalyst is so active already in the dark, with particular emphasis on the role of the support and its relation to the distribution and effects of adsorbed surface intermediates seen by *in situ* Fourier transform infrared (FTIR) spectroscopy.

The reverse water–gas shift (WGS) reaction plays an important role in CO_2 methanation, by providing the ruthenium with adsorbed carbon monoxide, CO_a, which is a primary reaction intermediate on the pathway to methane (*3*). Here we look in more detail at the relationship between the steady-state CO_2 methanation rate and metal-surface coverage by CO, for TiO_2 supports (namely Degussa P25 titania and the pure crystal phases, rutile and anatase), and for alumina for comparison.

Several articles appear in the literature pertaining to CO_2 methanation kinetics, mechanism, and surface intermediates for a wide range of supported noble metal catalysts. Solymosi *et al.* (*4*) reported a strong effect of support on CO_2 methanation over Rh. They observed the activity for $TiO_2 > Al_2O_3 > SiO_2$, and later reported the same

[1] To whom correspondence should be addressed at Sandia National Laboratories, Albuquerque, NM 87185.

[2] Current address: Paul Scherrer Institute, CH-5232 Wurenlingen, Switzerland.

0021-9517/91 $3.00

trend for Pd (*5*). These authors and others (*6*) have suggested a strong electronic effect of the support on the activity of the dispersed metal, with semiconductor properties being important in the case of TiO_2. Using dispersive *in situ* infrared spectroscopy, formate species were detected and appeared to exist mainly on the support. Furthermore, CO_a was detected and identified as a major metal-adsorbed intermediate (*5–7*). Due to the relatively low frequencies of IR bands attributed to CO_a, it was concluded that CO and atomic hydrogen are coadsorbed on the same metal site under reaction conditions.

Henderson and Worley (*6*) recently summarized many of the known features of CO_2 methanation, and the major points are briefly reiterated here. CO_2 hydrogenation is much more selective for CH_4 than is CO hydrogenation, the former reaction in general exhibiting a lower activation energy. In addition, CO_2 methanation occurs at such high rates that addition of gas-phase CO (CO_g) effectively inhibits the reaction. Yet, the mechanism involves some form of adsorbed CO (CO_a) in a pathway similar to that for CO_g methanation. Higher selectivities for CH_4, higher reaction rates, and lower reaction temperatures are thought to result from a favorable distribution of CO_a and adsorbed carbon species, C_a, during CO_2 methanation relative to CO_g methanation. A final point concerns the rate-limiting step(s) for the two reactions. CO_2 dissociation has been suggested as the rate-limiting step (*4*), however, the most popular belief is that CO_a dissociation or possibly C_a hydrogenation are the rate-limiting steps for both reactions (*5–8*). Both suggestions may be correct, since the rate-limiting step can be influenced by the metal, support, loadings, dispersion, temperatures, pressures, and reactant concentrations employed.

Here we focus our attention on CO_a, which is seen by diffuse-reflectance infrared Fourier transform spectroscopy (DRIFTS) on supported Ru catalysts during CO_2 methanation at temperatures between 100 and 190°C, and attempt to elucidate the overall involvement of this surface intermediate during the reaction at steady state.

MATERIALS AND METHODS

Catalyst Preparation

Ru, 3.8 wt%, on TiO_2 (Degussa P25, 55 m^2/g), rutile (Tioxide, 50 m^2/g) anatase (Tioxide, 65 m^2/g), and alumina (Degussa C, 100 m^2/g) were prepared by first dissolving 100 mg $RuCl_3 \cdot 3H_2O$ in 100 ml of 0.1 *M* HCl to which 1 g of the support was added after the initial solution was allowed to stabilize for 24 h. The pH of the suspension was slowly increased to 4.5 by adding 0.1 *M* NaOH. After evaporating the water off at 70°C, the solid was dried for 20 h at 170°C and then calcined for 12–18 h at 375°C. Residual NaCl was removed by dialysis over 4 days. The resulting catalyst was dried at 110°C and reduced in flowing 20% H_2 at 225°C for 1 h. This procedure yields a very active CO_2 methanation catalyst (±20% variation in activity from batch to batch), and when TiO_2 is the support, it is capable of producing methane from CO_2 and H_2 at temperatures as low as 50°C. Dispersions determined for the P25, anatase, and alumina samples by hydrogen chemisorption were 0.4, 0.45, and 0.2, respectively. Carbon, Cl, Na, and K impurity levels for the P25 sample were found to be 1000, 600 ± 100, 84 ± 8, and 25 $\mu g/g$, respectively.

Interestingly, in the case of Degussa P25, electron energy loss spectroscopy and transmission electron microscopy have verified that the Ru is preferentially deposited on the rutile component as 10–20 Å particles (*2, 9*) and in the case of pure rutile, it appears as a homogeneous paint-like coating (*10*).

Apparatus

DRIFTS continuous flow reactor. Flow experiments were carried out using two different configurations of the continuous DRIFTS/recycle reactor. This system consists of a heatable fixed-bed reactor coupled via an external recycle loop with a water trap (−30°C) and a controlled-environment

DRIFTS cell. Under normal conditions, the DRIFTS cell holds 70–100 mg of catalyst powder while 400–900 mg are loaded into the fixed-bed reactor. Two thermocouples, one located in the catalyst in the fixed bed and the other in the catalyst in the DRIFTS cell, are used with proportional-integral-derivative (PID) temperature controllers to ensure that *both* catalyst charges operate at the same temperature. An oscillating membrane pump maintains a flow rate of about 2 liters/min in the recycle loop, thus providing excellent backmixing in the reactor system when feed flow rates do not exceed 50 ml/min (25°C, 1 bar). A step-response tracer experiment produces an exponential, ideal stirred-tank response curve characterized by a mean residence time of 1.7 min for a feed rate of 50 ml/min. Uniform concentrations and matched temperatures as above ensure that infrared (IR) observations in the DRIFTS cell are representative of all the catalyst in the system (*3*).

Steady-state CO_2 methanation rates, R_{CH_4}, are obtained for any temperature, concentration vector, and reactant conversion level (<90%) through

$$m_c R_{CH_4} = \frac{y_{CH_4} F_i}{1 + 4y_{CH_4}}, \qquad (1)$$

where the methane mole fraction in the reactor (and in the reactor effluent), y_{CH_4}, is a measured variable, F_i is the total molar feed rate, and m_c is the catalyst mass. The denominator in Eq. (1) accounts for the nonequimolar reaction stoichiometry when all water produced in the reaction is trapped in the cold trap, which is the case for the operating condition used here (*3*). Also, the method of Weisz and Prater verified that all of the rate data presented herein fall well outside the regime influenced by internal and external mass transport limitations (*11*).

The second configuration for the continuous flow reactor simply involves bypassing the fixed-bed reactor and recycle loop and using the DRIFTS cell alone as a single-pass, differential reactor. All the data presented here that were obtained using this configuration correspond to CO_2 conversion levels that fall well below 1%.

Feed is supplied through one of two banks of mass flow controllers that can be selected using a low-volume, four-way switching valve across which pressure and flow rate are equilibrated to avoid surges during switching. Reactor effluent composition is determined with a Balzers QMG 420 quadropole mass spectrometer coupled with a two-stage continuous atmospheric sampling system. Quantitative data are obtained by regularly calibrating the mass spectrometer at $m/e = 15$ for CH_4, $m/e = 44$ for CO_2, and $m/e = 2$ for H_2 using the mass flow controllers to generate gas streams of known compositions. In all cases, reaction rates and reactant conversion are obtained from the effluent methane concentration and the known feed flow rates using Eq. (1). CO_2 and H_2 measurements are only used as a check on the overall material balance.

The DRIFTS cell (Harrick HVC-DRP vacuum chamber with DRA-2CO diffuse-reflectance accessory) is located in a Nicolet 710 FTIR spectrometer equipped with a midrange mercury–cadmium–tellurium (MCT) detector and a KBr beamsplitter. The instrument is operated at a scan speed of 1 scan/s and a resolution of 4 cm^{-1}. The number of coadded interferograms used to obtain a spectrum depends on signal intensity, which is a strong function of catalyst metal loading and support material, and typically ranges from 60 to 300 scans. Such operation results in data acquisition times for acceptable signal-to-noise ratios ranging between 1 and 3 min.

DRIFTS batch reactor. Batch experiments were carried out in a conventional vacuum manifold equipped with a liquid nitrogen trap, pressure measurement capabilities from 10^{-3} to 400 mbar, the facility for introducing premixed or pure gases, and a bulb-and-valve assembly for introducing controlled amounts of volatile liquids such as H_2O and formic acid (HCOOH). The manifold is evacuated using a liquid nitrogen

trap and a Balzers turbomolecular pump. It holds two catalyst samples, a large charge located in a temperature-controlled quartz bulb and a second much smaller charge loaded into a Harrick controlled-environment DRIFTS cell as described above. The DRIFTS cell is located in a BOMEM Michelson 110 (4 cm^{-1} fixed-resolution) FTIR spectrometer equipped with a narrow-range MCT detector and KBr beamsplitter. Preliminary checks of CO_g chemisorption dynamics showed a linear correlation of CO_a band area with global uptake, thus verifying that IR data from the DRIFTS cell truly represent the behavior of *all* of the catalyst in the system. Typically, 80 mg of catalyst is located in the DRIFTS cell and 400 mg in the quartz sample bulb, this larger charge being required for accurate quantitation in volumetric adsorption studies and as a useful check on relative methanation rate, which was monitored directly by FTIR.

Gases

CO_2 (99.995%), H_2 (99.9997%), and Ar (99.9997%) were used after passing through indicating Oxisorb oxygen traps which reduce oxygen impurity levels to less than 0.1 ppm. The use of high-purity gases is essential, especially for the diluent Ar, because even trace levels of CO_2 and H_2 impurities react on the catalyst to form CO_a, which accumulates in the case of continuous flow to the point that it becomes observable via FTIR spectroscopy. Furthermore, impurity oxygen can in certain cases adventitiously clean the surface of CO_a, giving the false impression of desorption into an inert carrier. These problems are less critical in the case of batch experiments, where much lower quantities of gas are involved. For those experiments, gases were used after applying several l-N_2 freeze–pump–thaw cycles to remove condensable contaminants.

Methods

Standard catalyst pretreatment consists of first heating the catalyst to 225°C in flowing 20% O_2 for 1 h followed by a brief purge in Ar and then reduction in 20% H_2 at 225°C for 1 h. The catalyst is then cooled to the planned reaction temperature in H_2 or Ar. This process was also used for regeneration between experiments, as it always brings the catalyst to its original level of methanation activity and CO_a coverage. Treatment of a used catalyst in O_2 yields CO_2 in the reactor effluent, suggesting the accumulation of carbon under reaction conditions. Within 15 min upon exposing a fresh or regenerated Ru/TiO_2 catalyst to the reaction mixture, methanation activity rises to a *quasi-steady-state*, then slowly falls to about 80% of its original value over a period of 4 h, after which it remains constant for a period of at least 96 h. All steady-state data are recorded during this latter period. The Ru/Al_2O_3 exhibits much slower dynamics and only reaches the quasi-steady-state (before onset of deactivation) after about 4 h.

Pretreatment plays a significant role in controlling the behavior of the catalysts for CO_2 methanation and in particular affects their abilities to support chemisorbed CO and surface formates. In preliminary work, direct reduction of the catalyst in H_2 at 225°C was found to yield reproducible initial methanation activity but, curiously, the CO_a band area was not nearly so reproducible. This observation, which has implications for the mechanism, is considered in some detail in the discussion section below.

IR spectra are presented in Kubelka–Munk (K–M) form

$$f(R(\nu)) = (1 - R(\nu))^2/2R(\nu), \qquad (2)$$

where f is the K–M function (dimensionless) and R is relative reflectance at wavenumber ν. The K–M function is the diffuse-reflectance analog to absorbance in transmission spectroscopy and varies linearly with the concentration of the absorbing species over a limited range of reflectance values. We assume here for simplicity that integral values of K–M band intensities (having the units of cm^{-1}) depend linearly on concentration. This assumption has been shown to be

reasonable for the type of data reported here (*3*). Relative reflectance is required in the K–M calculation, so it is necessary to make a proper choice for a reference spectrum. In most cases we use the reflectance spectrum for the clean catalyst in flowing 50% H_2 at the temperature of the experiment (background spectra depend strongly on temperature). For the batch experiments, the spectrum for pure KBr is used as the reference.

A judicious choice for the reference spectrum is important in quantitative work because we have observed that the shape of the background spectrum for the clean Ru/TiO_2 catalyst depends strongly on hydrogen concentration, possibly because of an electronic metal-support interaction mediated by hydrogen. Care must be taken in handling the relative reflectance spectra, as values surpassing 100% (which may arise in practice from experimental factors caused by variations in sample loading or position) are not meaningfully accommodated by the K–M transformation. Our experience has shown that reference spectra that are first multiplied by a large factor (20 or greater) provide the most reproducible and reliable band shapes and K–M integrals. Band integrals for CO_a are presented normalized to the value for the catalyst saturated with CO_a, obtained from CO_g adsorption at 110°C. These normalized integrals reflect the number of CO_a molecules relative to the total amount of CO that can be adsorbed, and hence represent fractional coverage (θ_{CO}).

IR characterization of surface adsorbates for the various catalysts was carried out in the single-pass DRIFTS reactor at 110°C, and a total flow rate of 50 ml/min (25°C, 1 bar). Steady-state kinetic experiments for determining methanation rate dependencies on temperature, H_2 mole fraction (y_{H_2}), and CO_2 mole fraction (y_{CO_2}) were carried out in the DRIFTS/recycle reactor by varying one parameter at a time while keeping the other two constant. For example, in a report of reaction rate versus y_{H_2}, the reactor feed concentrations were carefully adjusted with the mass flow controllers so that at each rate (i.e., at each conversion), y_{CO_2} was the same. In certain cases, conversions were so low that no feed adjustment was necessary. Steady-state reaction rates were calculated using Eq. (1), with y_{CH_4} being determined using the calibrated mass spectrometer. No hydrocarbons other than methane were ever detected.

Batch experiments in the vacuum manifold were used to compare the initial methanation rates and activities for formic acid dehydration, in addition to fractional coverages by CO_a for the different catalysts. Initial methanation rates were obtained by exposing the pretreated, evacuated catalyst at 150°C to a fixed mixture of CO_2 in H_2 (50 : 200 mbar) and then monitoring gas-phase methane in the precalibrated DRIFTS cell. Differential pressure measurements were used for quantitative verification of data thus obtained. Turnover numbers (TON) were calculated by incorporating the available number of Ru adsorption sites (as determined via CO_a adsorption in excess CO_g, assuming 1 : 1 CO : Ru stoichiometry, at 110°C). Fractional CO_a coverages (θ_{CO}) were obtained at steady state after 30 min in the CO_2 : H_2 mixture by normalizing the CO_a band integral by that seen for saturation coverage during the CO_g uptake experiment. Relative activities for CO_a formation were determined by introducing excess HCOOH (3 mbar) to the pretreated, evacuated catalyst at 100°C and monitoring the growth of CO_a via IR spectroscopy. Integrated CO_a band intensities were normalized against saturation CO_a coverage, as determined by subsequent exposure to excess CO_g (50 mbar) at the same temperature.

RESULTS

Identification of Adsorbed Intermediates

Figure 1 shows three spectra for the Ru/TiO_2 catalyst at 110°C taken in the single-pass DRIFTS cell. Figure 1a was recorded after exposing the pretreated catalyst to flowing CO_g (20%) for 1 h followed by a 5-min Ar purge to eliminate gas-phase

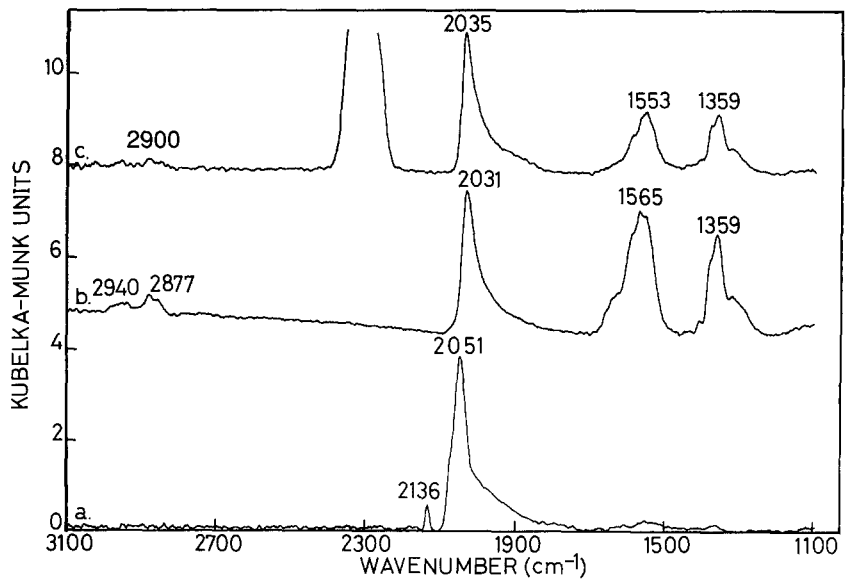

FIG. 1. DRIFTS Kubelka–Munk spectra for 3.8% Ru/TiO_2 in (a) Purged CO gas, (b) purged HCOOH, and (c) a 1 : 4 mixture of CO_2/H_2 at 110°C.

absorbance bands. The large band at 2051 cm^{-1} is characteristic of linearly bound CO on Ru (*6, 7, 12–15*). The small band at higher frequency (2136 cm^{-1}) is tentatively attributed to linearly adsorbed CO on Ru in a higher oxidation state, probably Ru^{3+}. Recent EPR studies of Ru on TiO_2, Al_2O_3, and SiO_2 showed that two types of Ru^{3+} species are generated during reduction in H_2, one associated with the support, and the other with RuO_x islands (*16*). The catalyst was then cleaned in flowing H_2 at 225°C until no CO_a species remained, cooled to 110°C, and then 2 μl of HCOOH was injected into flowing Ar carrier. After 15 min, spectrum 1b was obtained showing bands at 1565 and 1359 cm^{-1} arising from asymmetric and symmetric O–C–O stretching vibrations of adsorbed formate species (*4–7, 12*). The two small bands at 2940 and 2877 cm^{-1} are also known features of adsorbed formate. Although this interpretation is somewhat complex, it is generally agreed that the low-frequency band is the C–H stretch while the weaker, high-frequency band is probably a combination band involving the CO_2^- asymmetric stretch and C–H deformation (*4–7, 12, 17*). Also, a large feature at 2031 cm^{-1} is seen, which corresponds to CO_a, presumably formed via dehydration of HCOOH on or near active metal sites. Cleaning the catalyst in H_2 and cooling it to 110°C as above, followed by introduction of 10 mol% CO_2/40 mol% H_2 resulted, at steady state, in the continuous production of a very small amount of CH_4 (seen by mass spectroscopy), H_2O, and spectrum c in Fig. 1. Bands characteristic of formate are observed at 1359, 1553, and 2900 cm^{-1}, together with a large CO_a feature at 2035 cm^{-1}. For further confirmation of the importance of HCOOH (or $HCOO^-$) in the overall mechanism, the relative rates of CH_4 formation from CO_2/H_2 and $HCOOH/H_2$ mixtures were compared in the batch mode. As shown in Fig. 2, the initial rate (up to 20% conversion) from HCOOH is the same or slightly faster than from CO_2, as would be expected if the acid is an intermediate. Later deviations in the reaction rates may be related to the fact that HCOOH provides two of its own hydrogens whereas CO_2 does not provide any.

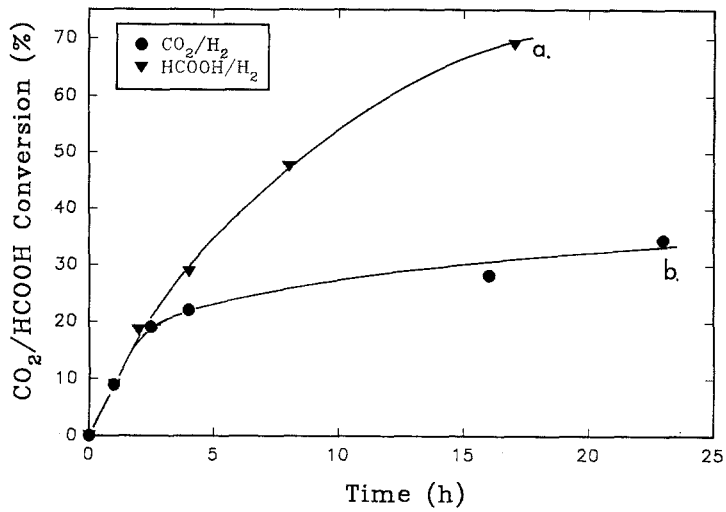

FIG. 2. Relative rates of CH_4 production at 170°C, 100 mbar from: (a) HCOOH : H_2 (1 : 7) and (b) CO_2 : H_2 (1 : 7) mixtures in the batch reactor as measured by *in situ* FTIR spectroscopy.

The interactions between CO_2, H_2, CO_a, and H_2O are reversible on the Ru/TiO_2 catalyst at 110°C as can be seen in Fig. 3, which shows what happens when a catalyst originally supporting CO_a (from CO_g) is exposed to sequential injections of liquid H_2O totalling 10 μl into the Ar carrier. The original CO_a (2041 cm^{-1}) reacts with water to form adsorbed formates (1548 and 1357 cm^{-1}) in addition to (bi)carbonates (1443 cm^{-1}) (*5, 12, 13*).

Identical experiments using CO_g, HCOOH, and the CO_2/H_2 mixture were also carried out on a blank P25 TiO_2 sample, which was treated according to the catalyst preparation procedure but without the addition of Ru. No adsorbed species were observed when the blank was exposed to CO_g or CO_2/H_2. When exposed to HCOOH, strong formate bands were seen at 1368, 1560, 2873, and 2940 cm^{-1}, but with no evidence for adsorbed CO. Negative bands appeared in the reference K–M spectrum at 3650, 3677, and 3733 cm^{-1} indicating that HCOOH reacts via condensation with surface hydroxyl groups forming water and adsorbed formate species. No desorption or decomposition of adsorbed formates occurred on the blank over a period of 4 h at 200°C in flowing Ar or H_2 gas streams. This result contrasts with observations for Ru/TiO_2, in which formate bands disappear in a flowing H_2 stream at temperatures as low as 80°C. The similarity between band shapes and positions over the blank and Ru/TiO_2 catalysts indicates that the formate species on the latter resides predominantly on the support. Hence, the lack of formates and CO_a from the CO_2/H_2 mixture over the blank shows that the metal plays a multifunctional role. It is necessary to catalyze CO_2 reduction to formate using metal-adsorbed hydrogen atoms. Formate then requires metal for dehydration (i.e., CO_a formation). Formate dehydration is probably driven by the stability of the CO_a species.

The high reactivity of formate species on the titania-supported catalyst parallels the CO_2 methanation activity for this catalyst and contrasts previous reports for alumina-supported Pd, Rh, and Ru (*12, 13, 18–21*). Figure 4 shows normalized integral band intensities for the 1359 cm^{-1} band seen in the single-pass DRIFTS cell for Ru/TiO_2 at 110°C experiencing a switch from steady state in 4 : 1 H_2 : CO_2 to dif-

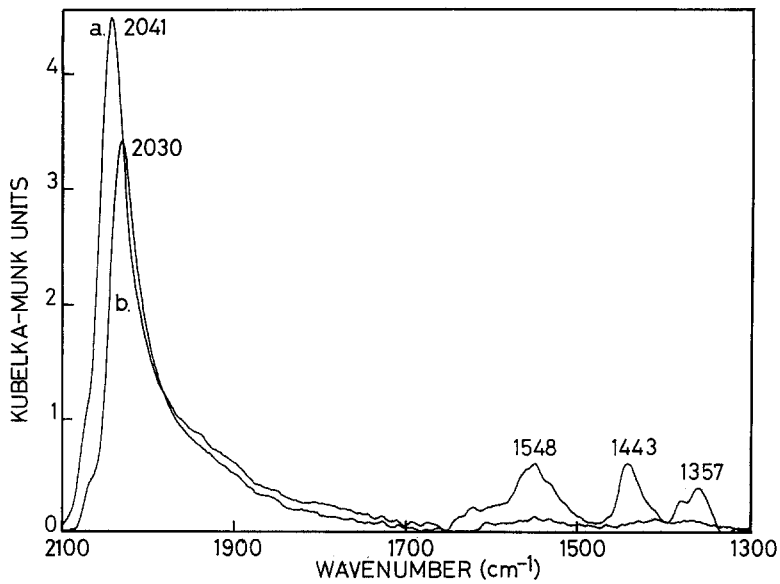

FIG. 3. DRIFTS Kubelka–Munk spectra for 3.8% Ru/TiO_2 in: (a) Purged CO gas and (b) after 1 h reaction with H_2O vapor at 110°C.

fering concentrations of H_2 in He. Methane was evolved during these experiments, but it is not known how much was due to reaction of formate since whenever formate is present, adsorbed CO is also seen. Interestingly, although H_2 is required for formate removal, large amounts seem to hinder the reaction. Similar behavior is observed when HCOOH is the source of adsorbed formate.

Figure 5 provides a more detailed look at the steady-state CO_a bands on Ru/TiO_2 from the DRIFTS reactor at 110°C for: (5a) the 1:4 CO_2/H_2 mixture at steady state, and (5b) from CO_g after purging. Both experiments form the same types of CO_a species, as indicated by the similarities in the IR spectra. The large band at 2043 cm^{-1} shifts to lower frequency with decreasing coverage. This trend is well known and has its origin almost certainly in dynamic and static CO–CO interactions (*22*). The ratio of the integrated band intensities between 2100 and 1700 cm^{-1} suggests a CO_a fractional coverage (θ_{CO}) during steady-state CO_2 methanation of about 0.4. This result, obtained in the single-pass mode, is entirely consistent with our earlier studies in the DRIFTS/recycle reactor combination (*3*).

Whereas CO_a species appear to be the same regardless of their source for the Ru/TiO_2 catalyst, this is not true for the Ru/Al_2O_3, for which typical IR spectra are shown in Fig. 6: (a) for a 1:4 $CO_2:H_2$ mixture and (b) for purged CO_g at 110°C. The heterogeneity in CO_a species is much greater in the case of Al_2O_3. Distinct IR bands occur at 1778, 1975, 2040, and 2139 cm^{-1} for the saturated catalyst (Fig. 6b) and at 1973, 2002, and 2048 cm^{-1} for the CO_2/H_2 mixture. The bands at 1778 and 1975 cm^{-1} are probably due to bridge-bonded CO_a (*13*) that at 2040 cm^{-1} corresponds to the linearly adsorbed species, and that at 2139 cm^{-1} may arise from Ru^{3+} as proposed above. In the methanation mixture, the band at 2002 cm^{-1} is attributed to the linearly adsorbed species at low coverage (*4–7, 12–14*). The other bands are harder to assign but the dominant band at 1973 cm^{-1} is probably bridge-bonded CO

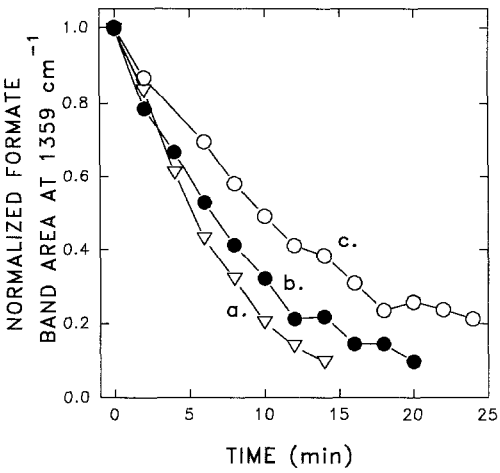

FIG. 4. Transient reaction of adsorbed formate on Ru/P25 at 110°C following a switch in feed concentration from steady state in 4 : 1 H_2 : CO_2 to: (a) 3.75 mol% H_2; (b) 6 mol% H_2; and (c) 25 mol% H_2 in He. Data are normalized K–M band integrals at 1359 cm^{-1} recorded in the single-pass DRIFTS cell.

as this would be formed first at lower coverages, while the band at 2048 cm^{-1} which is also discernible in spectrum 6b (high-coverage case) may represent linear CO on Ru in a low (but nonzero) oxidation state, i.e., Ru^+ or Ru^{2+}. It is important to mention that the alumina catalyst requires several hours to reach steady state at 100°C and is relatively difficult to clean, while the titania sample equilibrates rapidly (15 min) and is easily cleaned, even at 100°C. During methanation at steady state, CO_a occupies 20% of the available sites on Ru/Al_2O_3 in contrast to the value of 40% for Ru/TiO_2.

Steady-State Kinetic

Figure 7 shows reaction rate data in the Arrhenius form taken using the recycle reactor operated at steady-state concentrations of 10 mol% CO_2 and 40 mol% H_2. The gas composition was held constant by carefully adjusting the mass flow controllers to account for the influence of temperature on reactant consumption rates. CO_2 conversion never exceeded 75%. Both catalysts exhibit the same apparent activation energies, 19.3 ± 1 kcal/mol for Ru/TiO_2 and 19.1 ± 0.4 kcal/mol for Ru/Al_2O_3. However, the Ru/TiO_2 catalyst is consistently more active than the Ru/Al_2O_3 sample under the same conditions.

Steady-state kinetics were measured for the Ru/TiO_2 catalyst and are shown in Figs. 8 and 9. Methanation rate depends monotonically on hydrogen concentration at 120, 165, and 190°C. A log–log plot of all these data yields three lines of approximately the same slope, the average being 0.43 ± 0.05. Also shown in Fig. 8 are the DRIFTS-determined fractional coverages by CO_a, which were recorded concomitantly with the methanation rate measurements. The observation that θ_{CO} is constant at 120°C over the entire range of y_{H_2} indicates that the equilibrium value for θ_{CO} under these conditions is probably not perturbed by the methanation reaction, which is occurring very slowly due to the low temperature. Higher temperatures, and hence higher reaction rates reduce the steady-state CO_a reservoir, as seen

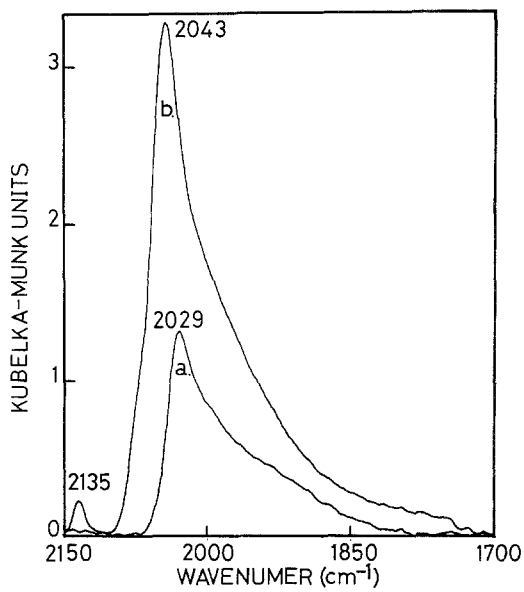

FIG. 5. DRIFTS Kubelka–Munk spectra of adsorbed CO on 3.8% Ru/TiO_2 in: (a) a 1 : 4 mixture of CO_2/H_2 and (b) purged CO gas at 110°C. Spectrum (b) represents complete coverage by adsorbed CO.

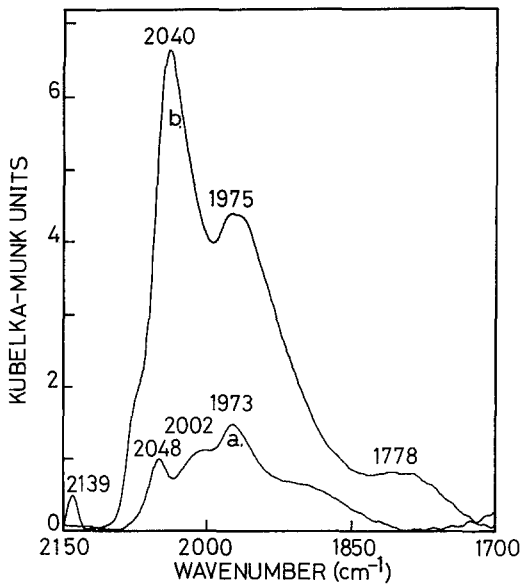

FIG. 6. DRIFTS Kubelka–Munk spectra of adsorbed CO on 3.8% Ru/Al_2O_3 in: (a) a 1 : 4 mixture of CO_2/H_2 and (b) purged CO gas at 110°C. Spectrum (b) represents complete coverage by adsorbed CO.

above 10 mol% H_2. Lower hydrogen concentrations reduce the methanation rate and hence the CO_a reservoir can build to higher levels.

Figure 9 shows reaction rate data as a function of CO_2 mole fraction for different temperatures and H_2 mole fractions. There is very little influence of y_{CO_2} on the methanation rate, and away from zero (where rate *must* be zero), the reaction appears to follow simple zero-order kinetics.

Batch Comparisons of Catalyst Activities

To better appreciate the effect of support on catalyst performance, batch DRIFTS experiments were performed on 3.8% Ru, supported on TiO_2 (P25), rutile, anatase, and Al_2O_3. The P25 and Al_2O_3 catalysts are from the same batches as those used for the experiments described above. Rutile/anatase mixtures were prepared in Degussa P25 proportions by stirring the powders together before loading them into the reactor. Table 1 presents the results from this study. Experiments were performed and analyzed as described in the sections on materials and methods with pretreatment applied when required between experiments.

These data show some remarkable features. First, there is a very strong support effect on TON, with a synergy evident for the anatase/rutile mixture that approaches the activity of P25. Second, there is no simple correlation between methanation activity and θ_{CO}. Third, activity toward HCOOH dehydration does not correlate with methanation rate, although the support clearly plays a role in this reaction as well. These results all suggest that formation of CO_a as measured by IR is not of rate-limiting importance for CO_2 methanation at low temperatures.

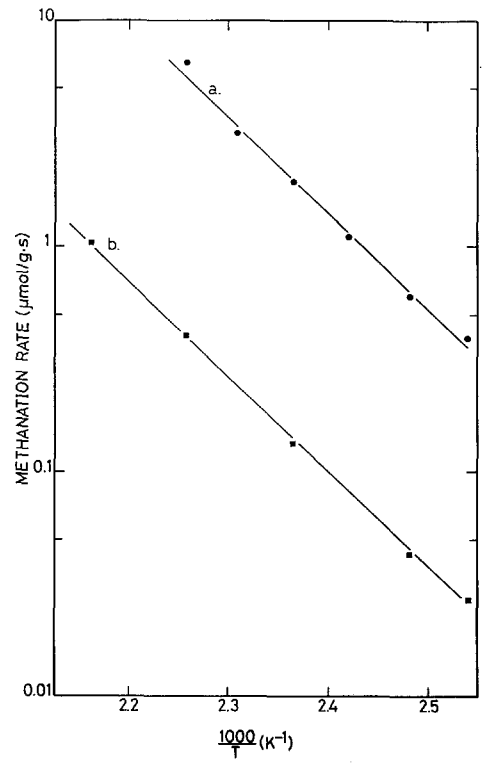

FIG. 7. Arrhenius plot of CO_2 methanation rate per gram of catalyst between 120 and 190°C for (a) 3.8% Ru/TiO_2, and (b) 3.8% Ru/Al_2O_3.

TABLE 1

Comparison of Catalytic Activities for CO_2 Methanation and CO_a Formation (by HCOOH Dehydration) for Several Catalysts

Catalyst 3.8% Ru on support	Initial CH_4 production rate at 150°C (μmol/g · s)	Available Ru (μmol)	θ_{CO} (30 min)	Initial turnover number $\times 10^3$ (s^{-1}) (150°C)	CO_a formation rate by HCOOH dehydration at 100°C (θ_{CO} after 15 min)
P25	6.7×10^{-2}	26	0.4	1.2	0.5
Anatase	1.7×10^{-2}	32	0.3	0.24	0.7
Rutile	3.3×10^{-2}	24	0.15	0.7	<0.05
TiO_2[a]	5.0×10^{-2}	28	0.15	0.9	0.8
Al_2O_3	8.0×10^{-4}	59	0.1	0.01	<0.05

[a] 4 : 1 mechanical mixture of anatase and rutile to simulate P25.

DISCUSSION

Based on the foregoing results, the following reactions are proposed to take place on the Ru/TiO_2 catalyst:

$$CO_{2(g)} \leftrightharpoons CO_{2(i)} \quad (1)$$

$$H_{2(g)} \leftrightharpoons 2H_{(m)} \quad (2)$$

$$CO_{2(i)} + 2H_{(m)} \leftrightharpoons HCOOH_{(i)} \quad (3a)$$

$$HCOOH_{(i)} \leftrightharpoons H^+_{(s)} + HCOO^-_{(s)} \quad (3b)$$

$$HCOOH_{(i)} \leftrightharpoons CO_{(m)} + H_2O \quad (3c)$$

$$CO_{(m)} + 6H_{(m)} \xrightarrow[\text{steps}]{\text{several}} CH_4 + H_2O \quad (4)$$

$$CO_2 + 4H_2 \rightarrow CH_4 + 2H_2O$$

where "m," "s," and "i" denote metal, support, and unspecified (possibly interfacial) adsorption sites. The possibility for formate mobility and accumulation on the support (step 3b) is demonstrated in Fig. 2, which shows $CO_{(m)}$ reacting with water to form formate species exhibiting IR band shapes and frequencies very similar to those seen from CO_2/H_2 mixture experiments on Ru/TiO_2 and from direct dosing of HCOOH on the blank TiO_2. This is in agreement with other workers who have concluded that formate species seen by IR during CO and CO_2 methanation (in addition to HCOOH adsorption) are predominantly located on the support or at the metal-support interface, rather than on the metal surface (*4–7, 12, 13, 18–21*). Furthermore, formate diffusion on the support and reaction at the metal-support interface has been implicated in the WGS reaction (*23*). It is still not clear, however, how hydrogen, although required for formate to react, also hinders the rate at which it reacts. It is possible that H_a blocks sites required for formate decomposition, but is required to remove decomposition products from the surface and prevent over accumulation. A similar argument has been proposed by Solymosi and Erdöhelyi (*24*) to explain how hydrogen inhibits HCOOH decomposition over supported Rh. Adsorbed hydrogen is specified (step 2), rather than H_2, since metal is required to catalyze the formation and decomposition of adsorbed formate species and the overall reaction kinetics exhibit half-order dependence on H_2 concentration. For simplicity, metal-adsorbed CO ($CO_{(m)}$) will henceforth be referred to as generic CO_a.

The CO_2 methanation activation energies found in this work for Ru/TiO_2 and Ru/Al_2O_3 fall in the range of reported values for supported noble metal catalysts, typically between 15 and 25 kcal/mol (*4–8, 25*). The fact that we observe the same value for

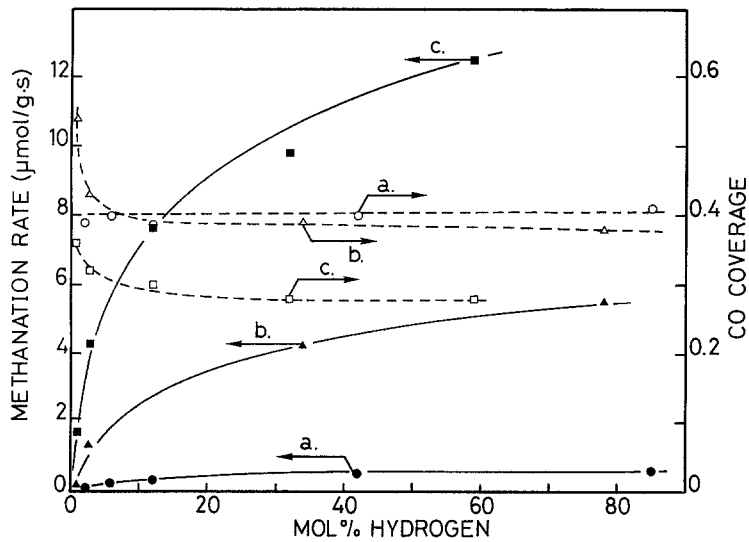

FIG. 8. Steady-state CO_2 methanation rate per gram of catalyst and fractional CO coverage dependence on molar hydrogen concentration at a fixed CO_2 molar concentration of 13% for 3.8% Ru/TiO_2 at (a) 120°C, (b) 165°C, and (c) 190°C.

both supported catalysts, for which metal loadings were similar, suggests that CO_2 methanation proceeds by the same mechanism in both cases, with the reaction rate being controlled by the same limiting step(s). Also, we observed that the Ru/TiO_2 surface equilibrates rapidly in the CO_2/H_2 mixture relative to that for Ru/Al_2O_3, and that CO_a is removed much more easily from the former by reaction with H_2. Thus, the support effect on methanation activity relates directly to the specific activity of the Ru metal, or the surface density of active sites, since there is little correlation of methanation rate with θ_{CO} or with formic acid dehydration activity (Figs. 3, 5, Table 1). As many Ru particles on TiO_2 are only 10–15 Å in diameter, compared to 25–30 Å on Al_2O_3 [2,9], a particle-size effect may be responsible for this difference.

For purposes of comparison, turnover numbers were calculated from the data in Fig. 7 using Ru dispersions of 0.4 and 0.2 for TiO_2 and Al_2O_3, respectively, and extrapolated to 200°C using the measured activation energies. At 200°C and a $H_2 : CO_2$ ratio of 4 : 1, the current TiO_2 and Al_2O_3 catalysts exhibit turnover numbers of 153×10^{-3} s^{-1} and 17×10^{-3} s^{-1}, respectively. This compares well with the finding of Solymosi *et al.* (*7*) of 13×10^{-3} s^{-1} (using their equation) for Ru on Al_2O_3.

The nearly one-half-order dependence of the methanation rate on H_2 mole fraction between 120 and 190°C implies that the rate-limiting processes depend to first order on H_a concentration, which is in equilibrium with gas-phase H_2 via a dissociative adsorption process. This conclusion is in good agreement with Cant and Bell (*26*) who observed that H_2 is in equilibrium with H_a during CO methanation even for CO coverages approaching unity.

It was demonstrated earlier via IR spectroscopy that CO_a can undergo methanation on Ru/TiO_2 during transient reaction with flowing H_2 at 120°C (*3*). However, the steady-state CO_a coverages of 0.4 and 0.2 seen for Ru/TiO_2 and Ru/Al_2O_3, respectively, at 110°C (Figs. 3 and 5) cannot explain the difference in reaction rates, especially in light of the results in Table 1, which show no correlation between TON and θ_{CO} for the different catalysts. This was further

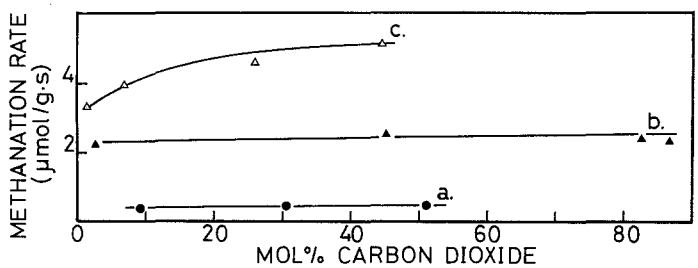

FIG. 9. Steady-state CO_2 methanation rate per gram of catalyst dependence on molar CO_2 concentration for 3.8% Ru/TiO_2 at (a) 120°C, 47 mol% H_2; (b) 165°C, 10 mol% H_2; and (c) 165°C, 47 mol% H_2.

emphasized in an interesting observation during an early steady-state experiment in which the normal methanation rate was seen for a Ru/TiO_2 catalyst (110°C) that exhibited only 2% coverage by CO_a (determined by IR). In contrast, formate IR bands were seen at their normal positions and intensities. The standard oxidation/reduction pretreatment followed by cooling to 110°C and introduction of the CO_2/H_2 mixture produced the normal methanation rate and the normal θ_{CO} = 0.4 CO_a IR band. It was later observed that catalysts in the state of abnormally low θ_{CO}, but normal methanation activity reproducibly generate significant quantities of CO_2 when heated in O_2, and rereduction always produces the original methanation activity and propensity to support CO_a. It is therefore concluded that the bulk of CO_a on Ru seen by IR spectroscopy during CO_2 methanation is predominantly a bystander to the reaction that mainly involves another adsorbed intermediate, possibly active carbon (*4–8, 13, 23, 27–30*) (or CO_a on a limited number of very active sites), and that many sites for CO_a can be blocked without affecting the overall methanation rate.

The lack of dependence of methanation rate on CO_2 partial pressure has not been previously reported; however, orders as low as 0.26 were seen for 5% Rh/Al_2O_3 (*4*). This zero-order behavior is probably a direct result of the buffering effect of the large CO_a reservoir, which in itself causes the methanation rate to be independent of θ_{CO}.

Table 1 shows that there is a strong effect of support on catalytic activity for HCOOH dehydration. However, this property correlates neither with the specific methanation activity (TON) nor with θ_{CO} during CO_2 methanation. Moreover, there is an interesting synergy for the rutile/anatase mixture. Individually, the specific methanation activity is higher for rutile than for anatase, but when mechanically mixed in 1:4 proportions (typical of Degussa P25), an even higher activity is achieved approaching that of the P25-supported catalyst. In contrast, Ru/P25 shows a HCOOH dehydration activity somewhere between that for rutile and anatase, whilst the mixture is dominated by the higher activity of the anatase component as expected. Furthermore, CO_a coverage for the mixture only reflects rutile behavior. Thus, it is likely that interparticle (i.e., bulk) mobility of intermediate species on the support plays an important role in HCOOH dehydration, CO_a accumulation and, eventually, in methanation activity. Alumina is greatly inferior to titania in all of its forms for these processes. However, the slow accumulation of CO_a on the Al_2O_3-supported Ru to a level not markedly lower than those typical of Ru/TiO_2 indicates that the very slow CO_a hydrogenation step is actually responsible for the overall poor performance of this catalyst.

Considering the difficulty of obtaining reproducible CO coverages without a careful catalyst pretreatment, the data suggest an unseen intermediate, possibly carbon, formed from CO_a but at a rate effectively

zero order in CO_a. This would be the case if a distinct heterogeneity of active sites exists. Even small levels of CO_a probably ensure that all of a limited number of a certain type of site are occupied by the active species so that the reaction proceeds only as a function of H_a concentration and temperature. In support of this idea, good evidence for heterogeneity in CO hydrogenation has already been reported from kinetic modeling studies (*31*). Furthermore, this reaction has been shown to be structure-sensitive over Ru (*32, 33*). When too much CO_a accumulates on the catalyst, as in the case of low-temperature CO_g methanation, reaction rate inhibition is observed (*3*). It is not yet known if this inhibition is due to H_a displacement or a lack of free sites necessary for CO_a dissociation.

Most CO_a seen by IR spectroscopy during CO_2 methanation is not reacting at steady state. However, during transient hydrogenation, all of the CO_a is able to migrate across the metal surface to the highly active sites where it is methanated quantitatively (*3*). At steady state, chemisorbed hydrogen must be available, first to enable CO_2 dissociation via the reverse WGS reaction of step 3 to form mobile CO_a species which migrate to fill the bulk surface CO_a reservoir, and second, to hydrogenate CO_a (and/or C_a) at a small number of especially active sites. This picture is identical to that proposed by Solymosi and co-workers (*5, 7*) except here we include reservoirs of CO_a and $HCOO^-$, which are not directly involved in the CO_a hydrogenation mechanism (step 4) to form methane.

CONCLUSIONS

The major conclusions from this work are summarized below:

1. CO_2 methanation proceeds on Ru/TiO_2 via adsorbed CO_a species, but methanation rate is insensitive to the concentration (θ_{CO}) of these species. Adsorbed CO_a is formed from the reverse water–gas shift reaction involving HCOOH as a major intermediate. The lack of correlation between θ_{CO} and methanation rate suggests a heterogeneous metal surface in which CO_a hydrogenation proceeds only on a small number of highly active sites. As a result, the reaction rate is insensitive to CO_2 concentration. At steady state, a large reservoir of CO_a ($\theta_{CO} = 0.4$) accumulates on the metal surface and provides CO to the active sites where it is hydrogenated in a multistep reaction sequence. It is this process which limits the steady-state reaction rate. Methanation rate depends on H_2 concentration to the one-half power indicating that the rate-limiting step requires adsorbed hydrogen atoms whose concentration depends primarily on adsorption equilibrium with gas-phase hydrogen.

2. The much higher activity of Ru/TiO_2 compared to Ru/Al_2O_3, despite their having identical activation energies and similar metal surface areas, suggests a greater density of active sites on the former.

3. Preliminary evidence suggests an enhancement of methanation rate when both anatase and rutile TiO_2 are present in the same (Ru-supporting) sample. The former appears to be more active in HCOOH dehydration (CO_a supply) while the latter is better for CO_a hydrogenation.

ACKNOWLEDGMENT

We are grateful to the Swiss National Fund for financial support.

REFERENCES

1. Thampi, K. R., Kiwi, J., and Grätzel, M., *Nature* **327,** 506 (1987).
2. Highfield, J. G., Ruterana, P., Thampi, K. R., and Grätzel, M., *in* "Structure and Reactivity of Surfaces" (C. Morterra, A. Zecchina, and G. Costa, Eds.), p. 469. Elsevier, Amsterdam, 1989.
3. Prairie, M. R., Highfield, J. G., and Renken, A. *Chem. Eng. Sci.* **46,** 113 (1991).
4. Solymosi, F., Erdöhelyi, A., and Bánsági, T., *J. Catal.* **68,** 371 (1981).
5. Erdöhelyi, A., Pàsztor, M., and Solymosi, F., *J. Catal.* **98,** 166 (1986).
6. Henderson, M. A., and Worley, S. D., *J. Phys. Chem.* **89,** 1417 (1985).
7. Solymosi, F., Erdöhelyi, A., and Kocsis, M., *J. Chem. Soc., Faraday Trans. 1* **77,** 1003 (1981).
8. Weatherbee, G. D., and Bartholomew, C. H., *J. Catal.* **87,** 352 (1984).

9. Ruterana, P., Thampi, K. R., Buffat, P.-A., and Grätzel, M. *Mater. Res. Symp. Proc.* **139,** 327 (1989).
10. Ruterana, P., Thampi, K. R., Buffat, P.-A., and Grätzel, M., *Ultramicroscopy,* in press.
11. Weisz, P. B., *Science* **179,** 433 (1973).
12. Dalla Betta, R. A., and Shelef, M., *J. Catal.* **48,** 111 (1977).
13. Kellner, C. S., and Bell, A. T., *J. Catal.* **71,** 296 (1981).
14. Robbins, J. L., *J. Catal.* **115,** 120 (1989).
15. Yokomizo, G. H., Louis, C., and Bell, A. T., *J. Catal.* **120,** 1 (1989).
16. Hobbis, C. M., Howe, R. F., Thampi, K. R., Kiwi, J., and Grätzel, M., unpublished results.
17. Buom, G., Lamotte, J., Lavalley, J.-C., and Lorenzelli, V., *J. Am. Chem. Soc.* **109,** 5197 (1987).
18. Robbins, J. L., and Marucchi-Soos, E., *J. Phys. Chem.* **93,** 2885 (1989).
19. Mirodatos, C., Praliaud, H., and Primet, M., *J. Catal.* **107,** 275 (1987).
20. Palazov, A., Kadinov, G., Bonev., Ch., and Shopov, D., *J. Catal.* **74,** 44 (1982).
21. Solymosi, F., Bánsági, T., and Erdöhelyi, A., *J. Catal.* **72,** 166 (1981).
22. Gughelminotte, E., Spoto, G., and Zecchina, A., *Surf. Sci.* **161,** 202 (1985).
23. Grenoble, D. C., Estadt, M. M., and Ollis D. F., *J. Catal.* **67,** 90 (1981).
24. Solymosi, F., and Erdöhelyi, A., *J. Catal.* **91,** 327 (1985).
25. Lunde, P. J., and Kester, F. L., *J. Catal.* **30,** 423 (1973).
26. Cant, N. W., and Bell, A. T., *J. Catal.* **73,** 257 (1982).
27. Estathiou, A. M., and Bennett, C. O., *Chem. Eng. Commun.* **83,** 129 (1989).
28. IIzuka, T., Tanaka, Y., and Tanabe, K., *J. Catal.* **76,** 1 (1982).
29. Masuda, M., and Miyahara, K., *Bull. Chem. Soc. Jpn.* **47,** 1058 (1974).
30. Winslow, P., and Bell, A. T., *J. Catal.* **91,** 142 (1985).
31. Ho, S. V., and Harriott, P., *J. Catal.* **64,** 272 (1980).
32. Vannice, M. A., *in* "Catalysis, Science and Technology" (J. R. Anderson and M. Boudart, Eds.) Vol. 3, Chap. 3 and references therein. Springer-Verlag, Berlin, 1982.
33. Shincho, E., Egawa, C., Naito, S., and Tamarta, K., *Surf. Sci.* **155,** 153 (1985).